Received: 13 March 2024 | Revised: 28 May 2024 | Accepted: 13 June 2024

DOI: 10.1002/alz.14122

Alzheimer's & Dementia®
THE JOURNAL OF THE ALZHEIMER'S ASSOCIATION

RESEARCH ARTICLE

Suppressing *UBE2N* ameliorates Alzheimer's disease pathology through the clearance of amyloid beta

Chen Zhang[1] | **Qingqing Jia**[1] | **Longhong Zhu**[1] | **Junqi Hou**[1] | **Xiang Wang**[1] | **Dandan Li**[1] | **Jiawei Zhang**[1] | **Yiran Zhang**[1] | **Su Yang**[1] | **Zhuchi Tu**[1] | **Xiao-Xin Yan**[2] | **Weili Yang**[1] | **Shihua Li**[1] | **Xiao-Jiang Li**[1] | **Peng Yin**[1]

[1]State Key Laboratory of Bioactive Molecules and Druggability Assessment, Guangdong Key Laboratory of Non-human Primate Research, Guangdong-Hongkong-Macau Institute of CNS Regeneration, Jinan University, Guangzhou, China

[2]Department of Anatomy and Neurobiology, Xiangya School of Medicine, Central South University, Changsha, China

Correspondence
Xiao-Jiang Li and Peng Yin, State Key Laboratory of Bioactive Molecules and Druggability Assessment, Guangdong Key Laboratory of Non-human Primate Research, Guangdong-Hongkong-Macau Institute of CNS Regeneration, Jinan University, 601 W. Huangpu Ave, Guangzhou, Guangdong 510623, China.
Email: xjli33@jnu.edu.cn and yinpeng177@163.com

Funding information
National Natural Science Foundation of China, Grant/Award Numbers: 32270564, 82394422, 82371874, 82271902, 82071421, 31500826; Guangzhou Key Research Program on Brain Science, Grant/Award Number: 202007030008; Department of Science and Technology of Guangdong Province, Grant/Award Numbers: 2021ZT09Y007, 2018B030337001; Guangdong Basic and Applied Basic Research, Grant/Award Numbers: 2022A1515011205, 2023A1515010811

Abstract

INTRODUCTION: Aging is one of the risk factors for the early onset of Alzheimer's disease (AD). We previously discovered that the age-dependent increase in Ubiquitin Conjugating Enzyme E2 N (UBE2N) plays a role in the accumulation of misfolded proteins through K63 ubiquitination, which has been linked to AD pathogenesis. However, the impact of UBE2N on amyloid pathology and clearance has remained unknown.

RESULTS: We observed the elevated UBE2N during the amyloid beta (Aβ) generation in the brains of 5×FAD, APP/PS1 mice, and patients with AD, in comparison to healthy individuals. *UBE2N* overexpression exacerbated amyloid deposition in 5×FAD mice and senescent monkeys, whereas knocking down UBE2N via CRISPR/Cas9 reduced Aβ generation and cognitive deficiency. Moreover, pharmacological inhibition of UBE2N ameliorated Aβ pathology and subsequent transcript defects in 5×FAD mice.

DISCUSSION: We have discovered that age-dependent expression of *UBE2N* is a critical regulator of AD pathology. Our findings suggest that UBE2N could serve as a potential pharmacological target for the advancement of AD therapeutics.

KEYWORDS
amyloid beta, cognitive behavior, pharmacological target, UBE2N

Highlights

- Ubiquitin Conjugating Enzyme E2 N (UBE2N) level was elevated during amyloid beta (Aβ) deposition in AD mouse and patients' brains.
- UBE2N exacerbated Aβ generation in the AD mouse and senescent monkey.
- Drug inhibition of UBE2N ameliorated Aβ pathology and cognitive deficiency.

Chen Zhang, Qingqing Jia, and Longhong Zhu contributed equally to this work.

1 | BACKGROUND

Aging is a time-dependent physiological process characterized by functional decline, and it represents a significant risk factor for various noninfectious diseases, including Alzheimer's disease (AD).[1,2] With the increasing aging population and the growing burden of health care for individuals with AD, research on this disease is expanding rapidly. AD is known to be associated with aging and is characterized by the presence of amyloid plaques and neurofibrillary tangles (NFTs), which are the major pathological hallmarks in the brain.[1,3,4] Although extensive research has focused on the biochemical mechanisms underlying the pathogenic events induced by misfolded amyloid beta (Aβ) and tau proteins, the exact cause of AD remains an open question. Studies have suggested a relationship between the ubiquitin-proteasome system (UPS) and Aβ generation,[5,6] particularly the abnormal binding of ubiquitin to Aβ, which can interfere with its clearance pathway. For example, Ayadi et al. found that ubiquilin-1 regulates amyloid precursor protein maturation and degradation by stimulating K63-linked polyubiquitination.[7] Duggan et al. described a coupling of ubiquitin conjungation to ER degradation (CUE) ubiquitin-binding domain in PS1, which mediates non-covalent binding to K63-linked polyubiquitin chains.[8] Paine et al. showed the immunocytochemistry presence of K63-linked polyubiquitin in a fraction of the NFTs in AD cortex, suggesting an active involvement of autophagy in the mechanism of AD.[9] Bellia et al. also identified that the N-terminal domain of the Aβ peptide interacts with the C-terminal tail of the K63-Ub, through its D1, E3, and R5 residues,[10] and that the folding stability of ubiquitin chains unexpectedly decreases with increasing chain length, resulting in the formation of amyloid-like fibrils.[11] Moreover, Puangmalai et al. demonstrated that the lysine 63–linked ubiquitination of tau oligomers contributes to the pathogenesis of AD,[12] and a mutant form of K63 ubiquitin also promotes the formation of tau- and superoxide dismutase 1 (SOD1)–positive inclusions selectively.[13]

The age-dependent accumulation of pathological proteins is believed to be a result of impaired cellular capacity to clear misfolded proteins.[14–16] Misfolded proteins are initially ubiquitinated and then targeted for degradation by the UPS or autophagy. We previously identified a role for the age-dependent elevated Ubiquitin Conjugating Enzyme E2 N(UBE2N) and impaired proteasome activity in senescent monkey synaptosomes,[17] which could contribute to the accumulation of misfolded Huntington's disease protein huntingtin (HTT) through preferential K63 ubiquitination. In addition, in mouse brain, age-dependent expression of UBE2N is also associated with impaired UPS activity and cytoplasmic accumulation of mutant TAR DNA-binding protein 43 (TDP-43).[18] However, the impact of UBE2N on Aβ pathology and clearance has remained unknown. In our current study, we observed the elevated levels of UBE2N during Aβ generation in the brains of 5×FAD mice, APP/PS1 mice, and patients with AD. Overexpression of *UBE2N* exacerbated Aβ deposition in the brains of 5×FAD mice and senescent monkeys, whereas deletion of *UBE2N* by CRISPR/Cas9 reduced Aβ generation and cognitive deficits, through the K48-linked ubiquitination degradation. It is notable that pharmacological inhibition of UBE2N ameliorated Aβ pathology in 5×FAD mice. Thus, we have identified *UBE2N*, an aging-related gene, as a critical regulator of AD pathology, and our findings also suggest that UBE2N could serve as a potential pharmacological target for advancement of AD medications.

RESEARCH IN CONTEXT

1. **Systematic review**: Aging is the most significant risk factor for the early onset of Alzheimer's disease (AD). We previously discovered that the age-dependent increase in Ubiquitin Conjugating Enzyme E2 N (UBE2N) plays a role in the accumulation of misfolded proteins through K63 ubiquitination, which has been linked to AD pathogenesis. However, the impact of UBE2N on amyloid pathology and clearance has remained unknown. In the current work, we detected the UBE2N level in AD mice and patients' brains, and then overexpressed UBE2N in 5×FAD mice and senescent monkey brain, or suppressed UBE2N by CRISPR-Cas9 or pharmacological inhibitor in 5×FAD mice.
2. **Interpretation**: We found elevated levels of UBE2N during Aβ generation in the brains of 5×FAD mice, APP/PS1 mice, and AD patients. Overexpression of *UBE2N* exacerbated Aβ deposition in the brains of 5×FAD mice and senescent monkeys, whereas deletion of *UBE2N* reduced Aβ generation and cognitive deficits. It is important to note that pharmacological inhibition of UBE2N ameliorated Aβ pathology in 5×FAD mice. Thus, aging-related increase in UBE2N, as a critical regulator of AD pathology, could serve as a potential pharmacological target for the development of AD drugs.
3. **Future directions**: The investigation of large animal models, closer to AD patients, would be highly valuable for understanding novel pathogenic mechanisms and identifying therapeutic targets. Lacking the large animal models of AD presents challenges and limitations due to the costly and time-consuming nature of such investigations. In addition, the manner of administration and pharmacological side-effects of UBE2N inhibitors remained to be understood. The species-related factors and the physiological safety of the drug, likely contribute to neurodegeneration, need to be further identified.

2 | METHODS

2.1 | Human brain specimens

Healthy and AD human brain specimens were obtained from the postmortem brains and peripheral tissues were obtained from the Brain

Bank of Xiangya School of Medicine through the willed body donation program. All brains were also assessed for optimal histological integrity and Alzheimer's-type neuropathology following a standard protocol proposed by the China Human Brain Banking Consortium.[19,20] The use of postmortem human brains was approved by institutional ethics committees, in compliance with the Code of Ethics of the World Medical Association (Declaration of Helsinki). For specimen information, please refer to Table S1.

2.2 | Animals

Cynomolgus monkeys were raised at Guangdong Landao Biotechnology Co. Ltd., an Association for Assessment and Accreditation of Laboratory Animal Care-accredited facility. Monkey health was monitored by veterinarians on a weekly basis, ensuring appropriate water, temperature, humidity, home cage conditions, and a day/night cycle. The 5×FAD, APP/PS1, and Cas9 mice were housed at the animal facility at Jinan University. Age-matched littermate mice, with gender randomization, were utilized for this study. All animal-related protocols were approved in advance by the Institutional Animal Care and Use Committee (IACUC) of Guangdong Landao Biotechnology Co. Ltd. and Jinan University. This study strictly adhered to the "Guide for the Care and Use of Laboratory Animals of the Institute of Laboratory Animal Science (est. 2006)" and "The use of non-human primates in research of the Institute of Laboratory Animal Science (est. 2006)" to ensure personnel safety and meet animal welfare requirements.

2.3 | Ethics approval

All animal-related experiments followed the National Institutes of Health (NIH) guide for the care and use of laboratory animals. Approval from the local ethical committee of Jinan University for animal experiments was obtained.

2.4 | Reagents

The primary antibodies used for western blotting, immunofluorescence, and immunohistochemistry were as follows: mouse anti-β-Amyloid (6E10) (BioLegend, 803001), rabbit anti-β-Amyloid (1-42) (D9A3A) (Cell Signaling Technology, 14974S), rabbit anti-K63 polyubiquitin (Cell Signaling Technology, 5621S), rabbit anti-K48 polyubiquitin (Cell Signaling Technology, 8081S), mouse anti-GAPDH (GeneTex, GTX100118), mouse anti-β-Actin (Protein-tech, 66009-1-Ig), rabbit anti-LC3B (Cell Signaling Technology, 2775S), mouse anti-UBC13 (4E11) (ThermoFisher, 37-1100), rabbit anti-UBC13 (Proteintech, 10243-1-AP), rabbit anti-NeuN (Abcam, ab177487), rabbit anti-GFAP (Abcam, ab7260), rabbit anti-Iba1 /AIF-1 (E4O4W) (Cell Signaling Technology, 17198S), mouse anti-Tau (Abcam, ab80579), mouse anti-phospho-Tau (AT8, ThermoFisher, MN1020), rabbit anti-PSD95 (Abcam, ab238135), rabbit anti-SNAP25 (Abcam, ab41455), and mouse anti-VCL/vinculin (Abcam, ab18058). Secondary antibodies included goat anti-mouse IgG (Boster, BA1051), goat anti-rabbit IgG (Boster, BA1055), Alexa Fluor 488 goat anti-mouse (Invitrogen, A11001), donkey anti-mouse Alexa Fluor 594, donkey anti-rabbit Alexa Fluor 488, and donkey anti-rabbit Alexa Fluor 594 antibodies from Jackson Immuno Research.

2.5 | Virus and vectors

The hUBE2N expressing vector, encoding human UBE2N, was generated previously using human cDNA and constructed in adeno-associated viruses (pAAV) 2-multiple cloning site (MCS) backbone for viral production at BamH1 and Xba1 restriction sites.[17,18] To generate the AAV2-U6-gRNA-cytomegalovirus(CMV)-red fluorescent protein (RFP) vector for mouse UBE2N in a CRISPR/Cas9 knocking-down experiment, the following gRNAs were expressed and based on PX552-RFP vector (Addgene, 60958): Target-1: 5′-GTAGGAAACCCAGCGTTTGCTGG-3′; and Target-2: 5′-TGGGGACCACTTATCTATGAAGG-3′. The polymerase chain reaction (PCR) product was inserted into the pCR2.1-TOPO vector using the TOPO TA Cloning Kit for target sequencing. The titers of AAV-UBE2N and AAV-gE2N target viruses, as well as the control viruses of AAV-green fluorescent protein (GFP) and AAV-gCtrl, were all confirmed by determining the number of packaged vector genomes using quantitative PCR.

2.6 | Method details

2.6.1 | Surgical procedure

The AAV2 viral injection into the monkey brain was performed following previously reported methods. In brief, each monkey was anesthetized with an intraperitoneal injection of 0.3–0.5 mg of atropine, followed by 10–12 mg of ketamine and 15–20 mg of PelltobarbitalumNatricum per kg body weight. The monkeys were secured on a stereotaxic instrument (RWD Life Science, 68901). The precise position for stereotaxic injection into the cortex was determined using MRI prior to the injection. Ten microliters of the target viruses was injected at different locations in the right brain, whereas the left brain was injected with the control virus, with the same depth of needle insertion calculated from preoperatively obtained MRI scans.

For injections into the mouse brain, the 5×FAD or 5×FAD;Cas9 crossing mice were anesthetized with intraperitoneal injection of 2.5% Avertin. Their heads were positioned in a stereotaxic instrument (RWD Life Science, 68801) equipped with a digital manipulator, a UMP3-1 Ultra pump, or a 10 μL Hamilton microsyringe. A 33 gauge needle was inserted through a 1 mm drill hole in the scalp. Injections were performed at the following stereotaxic coordinates: 2.0 mm posterior to bregma, 2.0 mm lateral to midline, and 2.0 mm ventral to dura, with the bregma set at zero. The microinjections were carried out at a rate of 0.18 μL/min. The microsyringe was left in place for an

additional 10 min before and after each injection. The target viruses (0.5 μL) of AAV-UBE2N or AAV-E2N gRNA, and the control viruses of AAV-GFP or AAV-control gRNA, were stereotactically injected into the hippocampus of the individual littermate mice.

The ALZET Brain Infusion Kit was used for the prolonged administration of NSC697923 for 4 weeks (at a constant rate of 0.11 μL/h, 535 ng/100 μL NSC697923 or vehicle control). After the anesthetization, a small incision was made in the mouse skin between the scapulae to separate the connective tissue to form a pocket, and a tiny osmotic pump was placed under the skin. The cannula was inserted into the right hippocampus of the mouse with the same stereotaxic coordinates. The skin incision was closed with sutures. Pathological tests were performed 1 month after implanting the cannulas, when treatment is concluded and the mice fully recovered from surgery.

2.6.2 | Recognition behavioral test

Three types of the recognition-associated behavioral tests were performed as the following sequence: novel object recognition test, T-maze test, and Morris water maze (MWM) test. There is a 1-day interval between the different types of behavioral tests.

The novel object recognition (NOR) test was conducted in a square cage measuring ≈50 cm × 50 cm × 50 cm. During the training phase, the mouse was given 10 min to explore two identical objects. On the test day, one of the objects was replaced with a novel object. The mouse was again allowed to explore the two objects for 10 min. The ratio of exploring time, spent between the old object and the novel object on the test day, was recorded for preference ratio calculation. During the whole NOR test, each mouse was tested randomly. The interval between the training phase and the test day is 24 h.

The T-maze test was performed using a T-shaped maze with three arms. The training phase lasted for 6 days. The goal arms were baited with reward food. The mice were placed in the maze for 3 min, three times a day, to familiarize themselves with the maze and consume the reward. On test day 7, one of the goal arms was blocked by a door, and the mouse was allowed to run from the start arm and consume all of the reward. Each mouse underwent 10 trials and the percentage of correct choices per mouse was calculated. During the whole T-test, each mouse was tested in random, with the minimum interval of 10 min.

The MWM test was conducted in a circular tank with a diameter of 120 cm, filled with opaque water maintained at 23°C. Four visual cues with different shapes were placed around the tank to assist the mice. The platform was submerged about 1.5 cm below the water surface and located in the southwest quadrant. During the training phase, the mice were placed in the other three quadrants randomly. The trials were conducted twice a day for 6 days, with a minimum interval of 10 min between trials. The mice were given 60 s to find the platform, and if they failed to find it within the allotted time, they were guided to the platform. After reaching the platform, the mice were allowed to stay on it for 15 s before being removed. The latency time to reach the platform was recorded using EthoVision XT (NoldUS). On the probe test day (day 7), the platform was removed, after which the time spent and swimming speed in the target quadrant were recorded.

2.6.3 | Open field test

The open field test was conducted in an empty square cage measuring ≈50 cm × 50 cm × 50 cm. The mice were placed in the cage randomly and were given 10 min to explore the field in free. The total distance and the velocity data were recorded and calculated by EthoVision XT (NoldUS).

2.6.4 | Immunoprecipitation and western blotting

For immunoprecipitation, a total of 500 μg brain tissues in cold 1% NP-40 buffer (50 mM Tris, pH 7.4, 50 mM NaCl, 0.1% Triton X-100, 1% NP-40 with 1× protease inhibitors and 100 μM PMSF) were precleared with protein A agarose beads (Sigma, P1406). Then the samples were immunoprecipitated by anti-β-Amyloid (6E10) at 4°C overnight. Protein A agarose beads were added to capture the target proteins for 2 h at 4°C. Ice-cold lysis buffer was used to wash beads three times. Proteins from the compound and input were subjected to western blotting and mass spectrometry. For western blotting, the brain tissues were homogenized in a soluble fraction buffer (10 mM Tris, pH 7.4, 100 mM NaCl, 1 mM EDTA, 1 mM EGTA, 0.1% SDS, 1% Triton X-100) containing protease inhibitors. The lysates were diluted in 1xSDS sample buffer and sonicated for 10 s after incubation at 100°C for 5 min. The total lysates (20 μg) were loaded onto a Tris-glycine gel and transferred to a nitrocellulose membrane. The western blotting was developed using the ECL Prime Chemiluminescence kit (GE Healthcare Amersham), and the band intensity of the soluble or aggregated β-amyloid labeled by antibodies (6E10, β-amyloid 1-42 or K63) was quantified by densitometry. Data were obtained from three independent western blotting tests.

2.6.5 | Immunofluorescence and immunohistochemistry

Mice were anesthetized with 5% chloral hydrate and perfused with 0.9% NaCl, followed by 4% paraformaldehyde (PFA). The brains were removed and postfixed in 4% PFA overnight at 4°C. The brains were then transferred to 30% sucrose for 48 h and cut into 20- or 40-μm sections using a cryostat at −20°C. Sections were blocked in 4% donkey serum with 0.2% Triton X-100 and 3% bovine serum albumin (BSA) in phosphate-buffered saline (PBS) for 1 h. For immunofluorescent staining, 20 μm sections were incubated with primary antibodies in the same buffer at 4°C overnight. After washing with 1x PBS, the sections were incubated with fluorescent secondary antibodies. For immunohisto-

chemistry with DAB staining, 40 μm sections were incubated with the antibody for at least 48 h at 4°C after pre-blocking. A biotin/avidin immuno-assay (Vector Laboratories) and DAB kit were used to visualize the staining. Images were acquired using a Zeiss microscope (Carl Zeiss Imaging, Imager A.2) with either a 10× or 20× lens (Plan-Neofluar 10×/0.3 or 20×/0.8) and a digital camera (Axiocam 506 color ZEISS) with ZEN 2.3 software.

To quantify immunofluorescent signals and Aβ plaque load, we used the method described previously.[21] In brief, using Image J (NIH) software and the Analyze tab, we chose the Set Measurements to select the Area, Area Fraction, and Limit to Threshold options. We then defined the region of interest (ROI) by outlining with the polygon function located on the toolbar. To quantify the amount of positive immunolabeling within the ROI, both "Area" (the total number of stained pixels within the ROI) and "Percent area" (the proportion of the ROI with positive labeling) were obtained. The percent staining for the combined ROI of the subregion in each section was calculated by adding the stained areas divided by the sum of the total areas. When all images for a specific animal had been quantified, the total percent staining across all sections was obtained, yielding the Aβ load.

2.6.6 | Proteasome activity assay

2.6.7 | Total RNA extraction and RNA sequencing

Fresh mouse brains were isolated for the RNA sequencing (RNA-Seq). Total RNA was extracted using TRIzol Reagent according to the manufacturer's protocol. The cDNA library was constructed, and sequencing was performed by Shanghai SANGO Company. The NEBNext Ultra RNA library prep kit for Illumina (E7530L; NEB) was used for sequencing following the manufacturer's recommendations. After cluster generation, the libraries were sequenced, and 150 bp paired-end reads were generated using the Illumina platform. Clean reads were obtained after discarding reads containing adapters, poly-N, or low-quality raw data. High-quality reads were aligned to the existing reference genome. The differentially expressed genes (DEGs) were chosen based on a fold-change > 1.5 and an adjusted p-value < 0.05. The Kyoto Encyclopedia of Genes and Genomes (KEGG) enrichment analysis for differentially expressed genes in a group was carried out using TBtools. The KEGG terms with a p-value < 0.01 and a hit rate > 0.05 were considered significantly enriched. In addition, principal component analysis and heat map visualization were also performed using TBtools.

2.7 | Statistical analyses

Statistical significance was assessed using the two-tailed Student's t-test when comparing two groups. One-way analysis of variance (ANOVA) was used to determine statistical significance when multiple groups were analyzed. Data were presented as mean ± SEM. Calculations were performed using GraphPad Prism software (GraphPad Inc.). A p-value < 0.05 was considered statistically significant.

2.8 | Data and materials availability

The key data supporting the findings of this study are presented within the article and the Supplementary Information. The RNA sequencing metadata are available at https://doi.org/10.6084/m9.figshare.24454177.

3 | RESULTS

3.1 | Elevation of UBE2N during Aβ deposition in the brains of AD mouse and patients with AD

Although extensive research has demonstrated the contribution of lysine 63–linked ubiquitination to the pathogenesis of AD, including its role in facilitating the formation of tau- and SOD-1-positive inclusions,[12,13] it remains unknown whether the age-dependent elevation of UBE2N is associated with AD pathology.[17,18] Thus, first, we compared the levels of UBE2N and K63 in hippocampal samples from 5×FAD−/− and 5×FAD+/− mouse littermates age 5–6 months. We found that both UBE2N and K63 were enriched in 5×FAD+/− mice with Aβ deposition (Figure 1A, B). Next, we examined whether the association of UBE2N-mediated K63 is age dependent in APP/PS1+/− mice. We observed a significant increase in the expression of UBE2N and K63 from middle age (5- to 6-months-old) to old age (10 to 12-months-old) during Aβ generation (Figure 1C, D). The immunoprecipitation of APP verified the increased K63 labeling in the brains of 5×FAD+/− and APP/PS1+/− mice (Figure S1). Furthermore, we confirmed the upregulation of UBE2N and K63 levels in the hippocampus of three AD patients compared to three non-AD control individuals, with postmortem brain samples collected within 24 h (Figure 1E, F and Table S1).

We also performed immunostaining of the mouse brains with UBE2N antibodies. Although the commercially available antibody to UBE2N reliably detected UBE2N on western blotting, its application for immunofluorescent double-labeling in the brains of WT mice did not yield robust and highly specific labeling. However, our investigation revealed increased UBE2N labeling in neuronal cells compared to glial cells in 5×FAD mice (Figure S2), which suggests that the UBE2N increase occurs primarily in AD neurons. Tau pathology is another important pathologic feature in AD. Although 5×FAD mice did not exhibit obvious tau accumulation,[22] and we were unable to observe the relationship between age-dependent increase UBE2N and tau in 5×FAD mice, examination of tau transgenic mice expressing mutant tau (P301S) also revealed that UBE2N was increased in the hippocampus of tau (301S) mice (Figure S3). Thus, UBE2N is likely to be elevated during aging and under other pathological conditions.

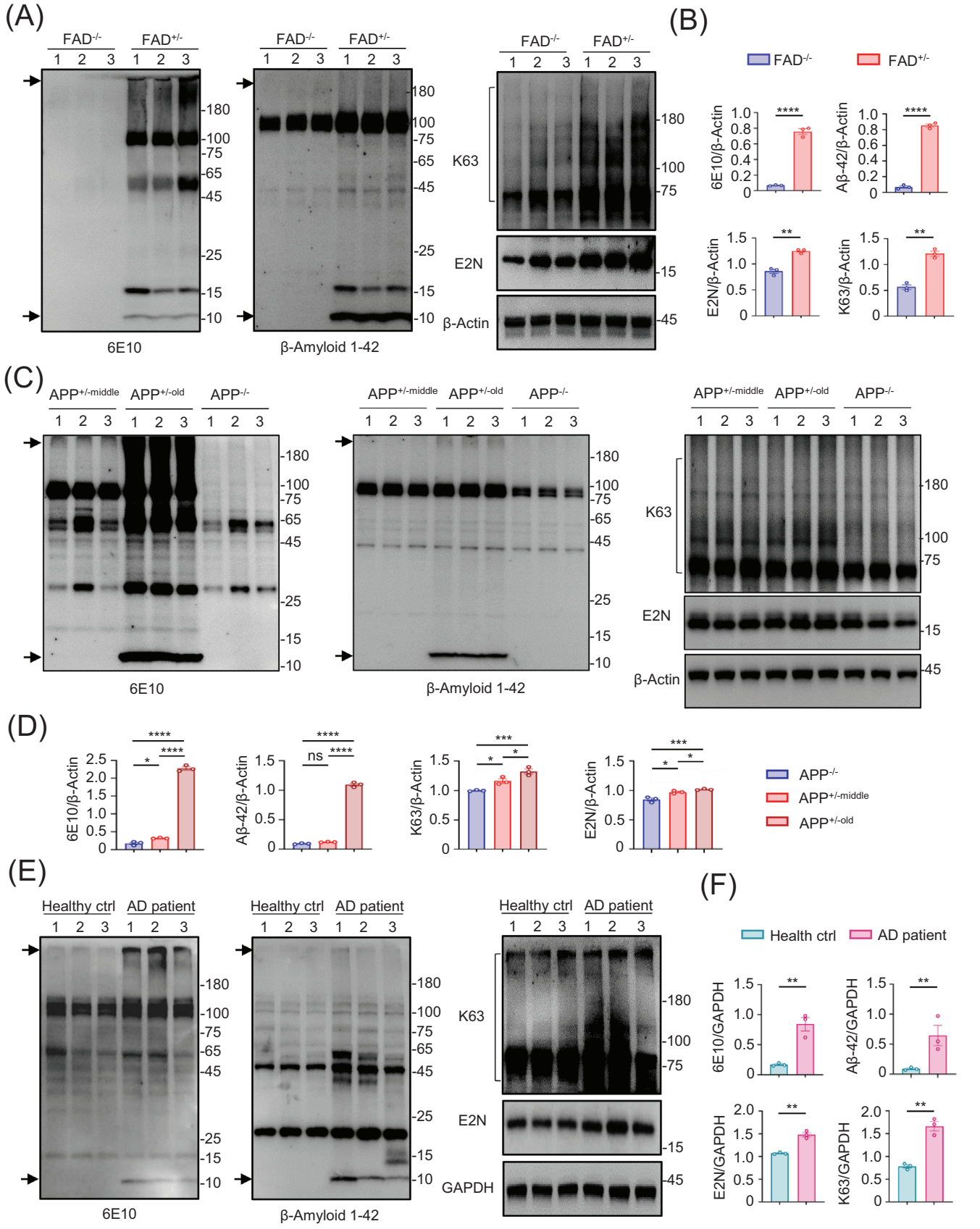

FIGURE 1 *Ubiquitin Conjugating Enzyme E2 N (UBE2N)* expression is associated with amyloid beta (Aβ) deposition in the brains of 5×FAD and APP/PS1 mice and patients with Alzheimer's disease(AD). (A) Western blotting analysis of Aβ deposition, UBE2N, and K63 in the hippocampal samples from three 5×FAD−/− and three 5×FAD+/− mice. The arrow indicates the aggregated or monomer Aβ bands. (B) Quantitative

3.2 | Overexpression of UBE2N promoted Aβ pathology and cognitive deficiency in 5×FAD mice

Considering that UBE2N is an E2 conjugating enzyme that selectively mediates the elongation of K63-linked polyubiquitin chains,[23–25] and that increased UBE2N has been implicated in various pathological conditions, such as promoting the accumulation of misfolding mutant HTT and TDP-43 proteins,[17,18] we aimed to determine the mechanism by which UBE2N affects Aβ pathology and clearance through K63-polyubiquitin modification. We constructed AAV2 virus vectors expressing UBE2N or GFP under the CMV promoter (Figure 2A) and injected them into the hippocampus of 5- to 6-month-old 5×FAD mice. After 1 month, we conducted a series of cognitive behavior tests (Figure 2B, C, and S4A), including MWM, NOR, and T-maze. We observed that compared to 5×FAD mice expressing AAV-GFP control, the injection of AAV-UBE2N resulted in exacerbated spatial memory ability, as indicated by the increased latency time to platform. Although *UBE2N* overexpression reduced the swimming performance of 5×FAD mice, track traces of mouse walking and the open field test did not reveal any obvious motor function deficits (Figure S4B), consistent with the notion that impaired recognition abilities could also compromise the swimming abilities of the mice.[26,27] Western blotting analysis revealed the increased accumulation of aggregated or dimeric Aβ in the brains of 5×FAD mice with *UBE2N* overexpression (Figure 2D, E). Immunofluorescent (Figure 3A, B) and immunohistochemical (Figure 3C, D) staining confirmed the presence of more Aβ aggregates, detected by 6E10 or Aβ 1-42 antibodies, in the hippocampus of 5×FAD mice expressing AAV-UBE2N compared to AAV-GFP control.

3.3 | Overexpressing *UBE2N* exacerbated Aβ generation in the senescent monkey brain

The non-human primate (NHP) model of AD has been used frequently to demonstrate that elderly animals develop early AD-like pathologies, including the accumulation of Aβ plaques and hyperphosphorylated tau.[28] For instance, studies have shown diminished cognitive abilities in senescent monkeys,[29–31] along with decreased brain volumes, increased cerebral Aβ burden, and cerebral glucose hypometabolism.[32–36] To confirm the involvement of UBE2N in Aβ pathology in the NHP brain, we constructed the AAV-BRI-Aβ42 virus vector, which expresses artificial Aβ42 under the (ubiquitin C) UBC promoter (Figure 4A). We co-injected this vector with AAV-E2N into the right-side cortex of 7- to 9-year-old WT cynomolgus monkeys, while the opposite left-side cortex of same monkey was co-injected with AAV-BRI-Aβ42 and AAV-GFP control. After 2 mo of virus expression, the overexpression of UBE2N led to a significant accumulation of exogenous aggregated Aβ or BRI-Aβ42, but without generation of the endogenous monomer Aβ bands, compared to the GFP control (Figure 4B, C). Immunofluorescent staining of the monkey cortex using 6E10 or Aβ 1-42 antibodies revealed that more Aβ aggregates were generated in the hippocampus of the AAV-BRI-Aβ42 expressing monkey cortex, when co-injected with AAV-E2N than with AAV-GFP (Figure 4D, E). In addition, we injected AAV-E2N or AAV-GFP alone into the right or left cortex of cynomolgus monkeys at different ages, respectively, to exclude individual differences. Of interest, immunohistochemical staining with an antibody to Aβ 1-42 showed that the aggregated Aβ plaques were only enriched in the cortex of old-age cynomolgus monkeys (21–23 years) injected with AAV-E2N, but not in the middle-aged monkeys (7–9 years) or AAV-GFP controls (Figure 4F). To confirm that overexpressing *UBE2N* exacerbates Aβ accumulation in the senescent monkey brain, we performed western blotting analysis, and also found that the dimer Aβ was increased significantly only in the cortex of old-age monkeys with AAV-E2N, but not in middle-aged monkeys or GFP control groups (Figure 4G, H).

Tau pathology was found in cynomolgus monkeys at the age of 36 years.[37] We did not observe that AAV-E2N could increase phosphorylated tau in the cynomolgus monkeys at 21–23 years of age (Figure S5). This suggests that a longer aging process may be necessary for the development of tau pathology in the brains of these monkeys.

3.4 | Deletion of *UBE2N* reduced Aβ generation and cognitive deficiency in 5×FAD mice

Considering the current observation that overexpressing *UBE2N* exacerbates Aβ generation and cognitive deficiency, we hypothesized that suppressing endogenous UBE2N levels could ameliorate AD pathology through the UPS clearance of amyloid. Most studies have reported the role of K48-polyubiquitin chain signaling in proteasome-mediated

representation of band intensity for the aggregated Aβ smear bands of 6E10, Aβ 1-42, UBE2N, or K63. Data were obtained from three independent western blotting analyses of 5×FAD−/− and 5×FAD+/− hippocampal tissues. Data are presented as mean ± SEM and analyzed using unpaired Student's *t*-test ($n = 3$ mice per group, 5- to 6- months-old, ****: $p < 0.0001$; **: $p < 0.01$). (C) Western blotting analysis of Aβ, UBE2N, and K63 in three APP−/− mice and three age-dependent APP+/− mice. The middle APP+/− represents 5- to 6-month-old mice, whereas old APP+/− indicates 10- to 12-month-old mice. The arrow indicates the aggregated or monomer Aβ bands. (D) Quantitative representation of band intensity for the aggregated Aβ smear bands of 6E10, Aβ 1-42, UBE2N, or K63. Data obtained were from three independent western blotting analyses ofAPP−/−, middle APP+/−, and APP+/− mouse hippocampus tissues. Data are presented as mean ± SEM and analyzed using one-way ANOVA with Tukey's test. ($n = 3$ mice per group, ****: $p < 0.0001$; ***: $p < 0.001$; *: $p < 0.05$; ns: not significant) (E) Western blotting analysis of Aβ, UBE2N, and K63 in three AD patients and three non-AD control individuals. The arrow indicates the aggregated or monomer Aβ bands. (F) Quantitative representation of band intensity for the aggregated Aβ smear bands of 6E10, Aβ1-42, UBE2N, or K63. Data were obtained from three independent Western blotting analyses of tissues of AD patients and non-AD control individuals. Data are presented as mean ± SEM and analyzed using unpaired Student's *t*-test ($n = 3$ samples per group, **: $p < 0.01$).

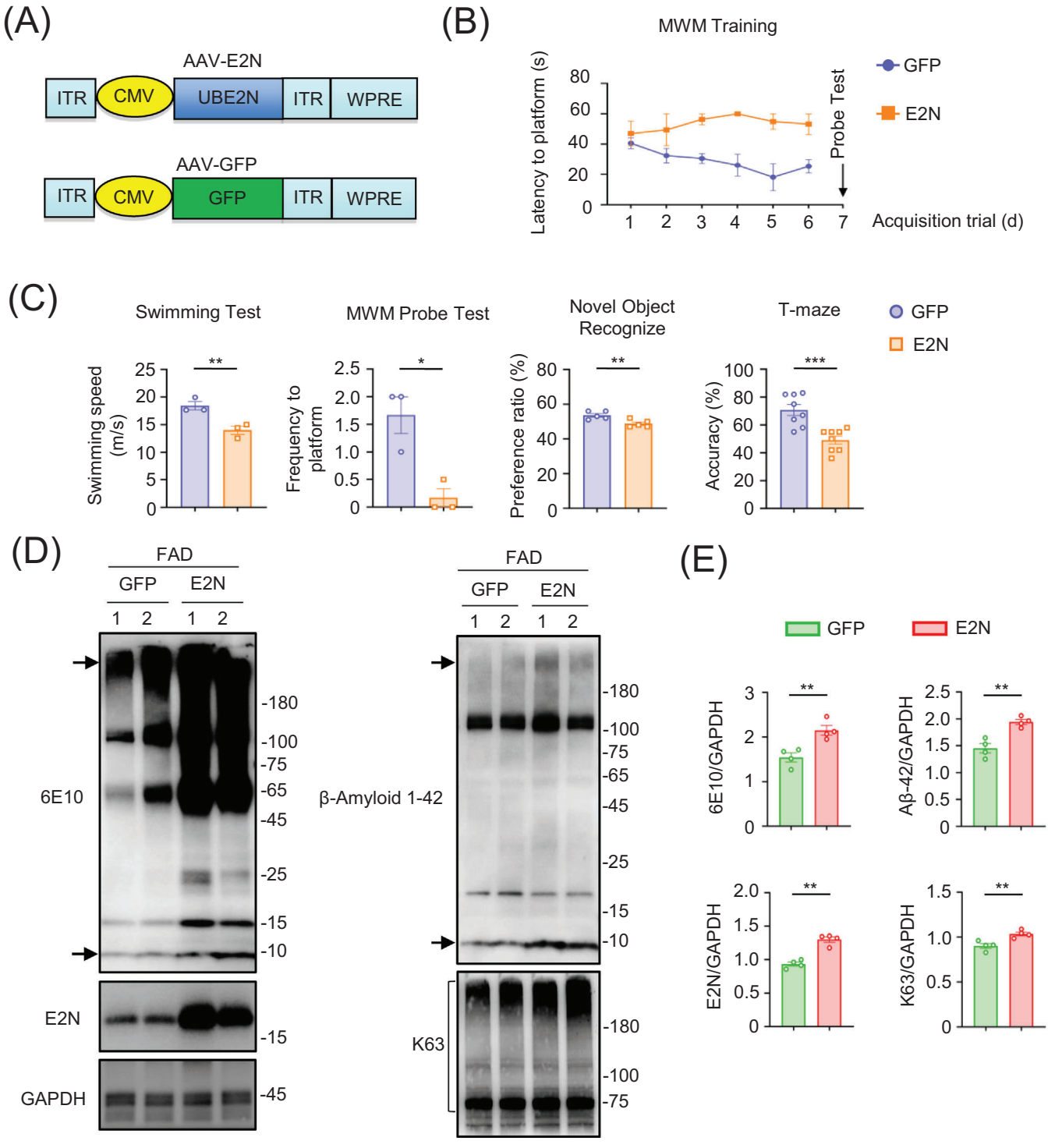

FIGURE 2 Overexpression of *UBE2N* promotes Aβ generation and cognitive deficiency in 5×FAD mice. (A) Construction of adeno-associated virus (AAV)2 virus vectors expressing UBE2N or green fluorescnet protein (GFP) under the cytomegalovirus (CMV) promoter. (B) Morris water maze (MWM) test results showed the latency time to reach the platform, a measure of spatial memory, in 5×FAD mice injected with AAV-E2N as compared to mice expressing AAV-GFP ($n = 8$ mice per group, 5- to 6-months-old). (C) The swimming speed and the frequency to platform number in the MWM probe test of 5×FAD mice with overexpression of AAV-E2N compared to AAV-GFP control. The preference ratio in the novel object recognition test, and the accuracy result in T-maze as measures of memory ability between AAV-E2N- and AAV-GFP- injected 5×FAD mice. Data are presented as mean ± SEM and analyzed using unpaired Student's *t*-test ($n = 8$ mice per group, 5- to 6-months-old, ***: $p < 0.001$, **: $p < 0.01$, *: $p < 0.05$). (D) Western blotting analyses of 6E10, Aβ 1-42, UBE2N, and K63 in two 5×FAD mice injected with AAV-E2N or AAV-GFP control. The arrow indicates the aggregated or monomer Aβ bands. (E) Quantitative representation of band intensity for 6E10, Aβ 1-42, UBE2N, and K63. Data were obtained from 5×FAD mouse hippocampus injected with AAV-E2N and AAV-GFP control. Data are presented as mean ± SEM and analyzed using unpaired Student's *t*-test ($n = 4$ mice per group, 5–6 months old, **: $p < 0.01$).

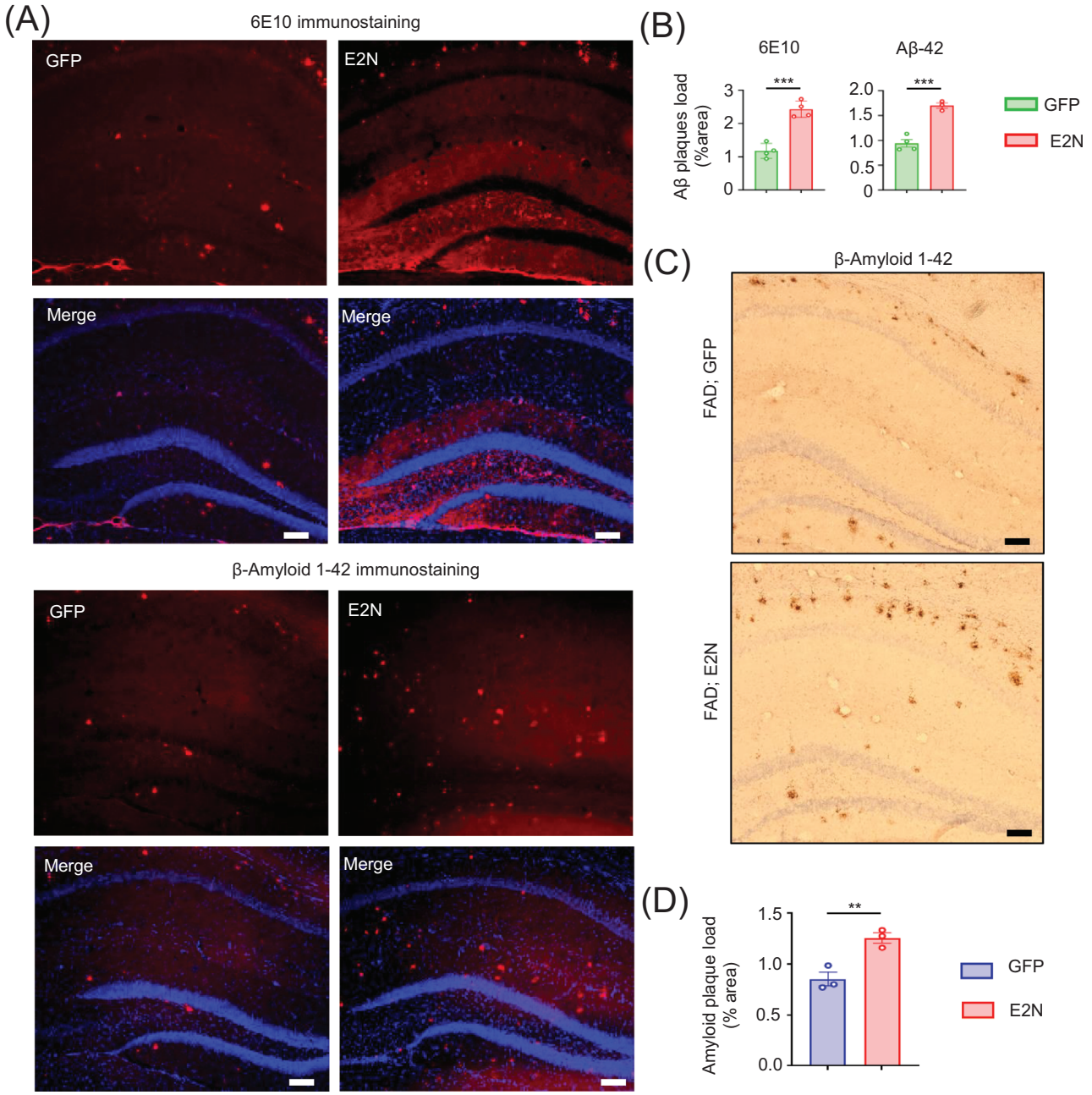

FIGURE 3 Overexpression of *UBE2N* exacerbates Aβ pathology in 5×FAD mice. (A) Immunofluorescent staining of the hippocampus in 5×FAD mice injected with AAV-E2N or AAV-GFP control. Aβ aggregates (red color) were detected using 6E10 or Aβ 1–42 antibodies, and the nuclei were stained with DAPI (blue color). Scale bars: 100 μm. (B) Quantification of amyloid plaques stained by 6E10 or Aβ 1–42 antibodies in the hippocampus of 5×FAD mice expressing AAV-E2N or AAV-GFP. Data presented as mean ± SEM, analyzed using unpaired Student's *t*-test ($n = 4$ mice per group, 5- to 6-months-old, ***: $p < 0.001$). (C) Immunohistochemical staining with the antibody to Aβ 1–42 indicating Aβ plaques in the hippocampus of 5×FAD mice injected with AAV-E2N or AAV-GFP control. Scale bar: 100 μm (D) Quantitative analysis of the Aβ plaques (the average optical density). Five random fields (20X) in each slice from three animals in each group were used to generate data. The data are presented as mean ± SEM and analyzed using unpaired Student's *t*-test (**: $p < 0.01$).

protein degradation, whereas K63-polyubiquitin conjugates are involved in a non-UPS pathway.[38] In this study, we used guide RNA sequences to target mouse *UBE2N* located in exon 2 or exon 3 sites, while the scramble sequences without any target genes as a control. These sequences were inserted into the AAV2-PX552-RFP vector to express E2N gRNAs under the U6 promoter, and the RFP fluorescent protein under the CMV promoter (Figure 5A). We then injected the E2N gRNAs virus into the hippocampus of 5- to 6-month-old 5×FAD/Cas9 mice, which express Cas9 by crossing 5×FAD mice with the transgenic Cas9 mice. Immunofluorescent double staining verified the efficient infection of neuronal and glial cells in the viral injected mouse brains (Figure 5B). Through TA cloning and sequencing,

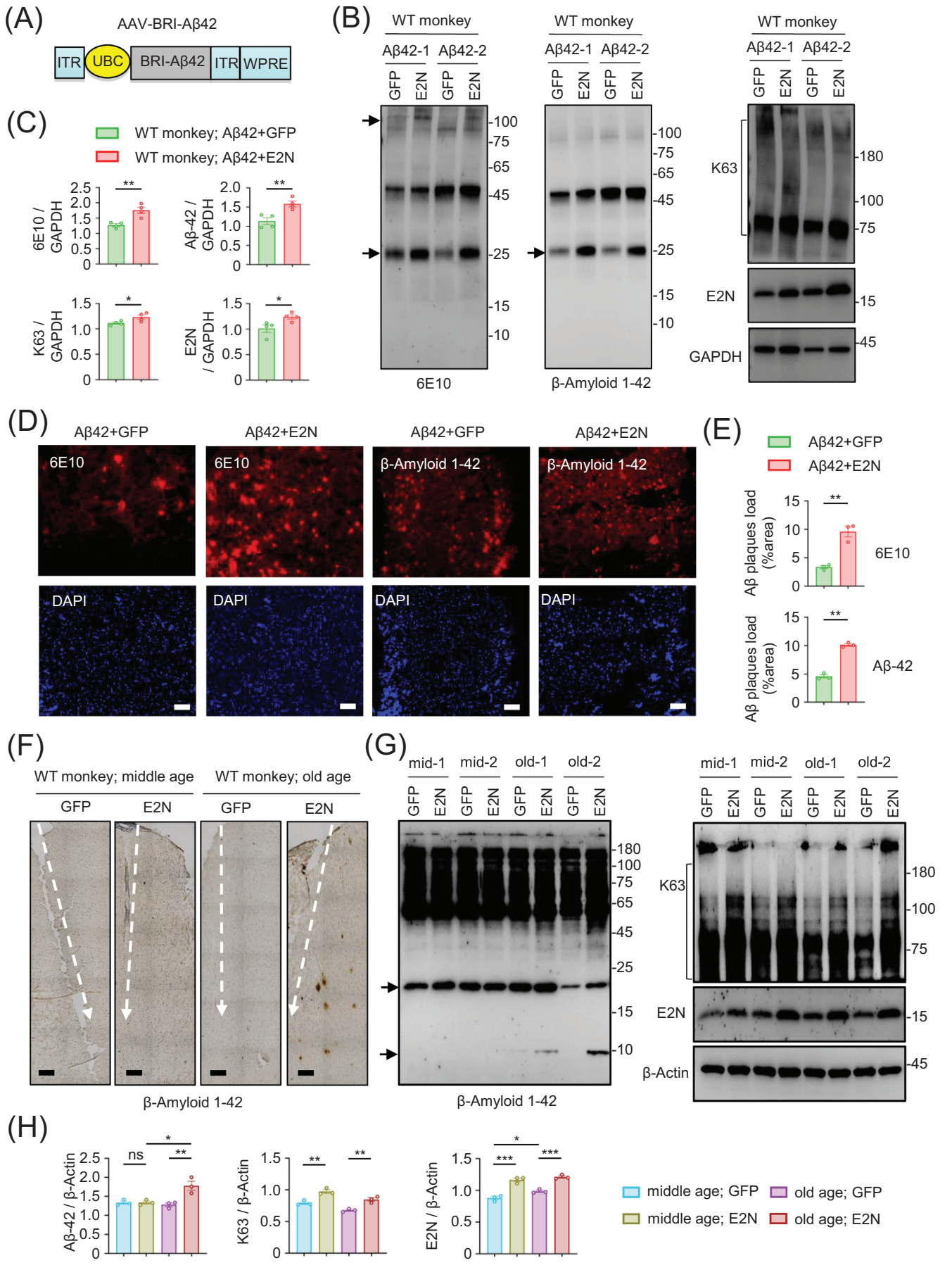
(A)
AAV-BRI-Aβ42
ITR
UBC
BRI-Aβ42
ITR
WPRE
(B)
WT monkey
Aβ42-1
Aβ42-2
GFP
E2N
6E10
β-Amyloid 1-42
K63
E2N
GAPDH
(C)
WT monkey; Aβ42+GFP
WT monkey; Aβ42+E2N
6E10 / GAPDH
Aβ-42 / GAPDH
K63 / GAPDH
E2N / GAPDH
(D)
Aβ42+GFP
Aβ42+E2N
6E10
β-Amyloid 1-42
DAPI
(E)
Aβ plaques load (%area)
6E10
Aβ-42
(F)
WT monkey; middle age
WT monkey; old age
GFP
E2N
β-Amyloid 1-42
(G)
mid-1
mid-2
old-1
old-2
K63
E2N
β-Actin
β-Amyloid 1-42
(H)
Aβ-42 / β-Actin
K63 / β-Actin
E2N / β-Actin
middle age; GFP
old age; GFP
middle age; E2N
old age; E2N

we verified the mouse *UBE2N* genome editing, evidenced by the truncations of *UBE2N* DNA mediated by CRISPR/Cas9 targeting (Figure S6). After 1 month, we conducted cognitive behavior tests, including MWM (Figure 5C, D). We confirmed that the injection of AAV-E2N gRNA partially alleviated the latency time to platform, which attenuated the loss of spatial memory ability, compared to the 5×FAD/Cas9 mice expressing the non-target control. Western blotting analysis also indicated a decrease in the aggregates or dimer Aβ upon knocking down *UBE2N*. Furthermore, the K48 ubiquitination level was increased, while the K63 polyubiquitin was significantly inhibited, without any alteration in the autophagy marker LC3 (Figure 6A, B). The proteasome is a large multi-catalytic protease complex involved in many highly regulated processes. It has three major catalytic activities: a chymotrypsin-like activity, a trypsin-like activity, and a post-glutamyl peptide hydrolyzing activity.[39] Consequently, we found that the chymotrypsin-like and post-glutamyl activities of UPS were statistically increased by the injection of AAV-E2N gRNA compared to AAV-control gRNA (Figure 6C). In addition, immunofluorescent staining confirmed the clearance of Aβ aggregates in the hippocampus of 5×FAD/Cas9 mice when expressing AAV-E2N gRNA (Figure 6D, E).

3.5 | Pharmacological inhibition of *UBE2N* ameliorated Aβ pathology in 5×FAD mouse

Given that the deletion of *UBE2N* can reduce Aβ generation and cognitive deficiency in the 5×FAD mouse, finding a suitable small molecule, pharmacological drug targeting UBE2N may provide a potential strategy for AD therapeutic agents. NSC697923 is a potent UBE2N inhibitor with limited application in human diseases, including its antitumor activity.[40–42] To explore the potential pharmacological influence of this UBE2N inhibitor, NSC697923, on misfolded Aβ plaque, we delivered it into the hippocampus of 5×FAD mice using Alzet Pump infusion for 4 weeks (Figure 7A). The matched 5×FAD littermates were strictly treated with a vehicle solution containing DMSO for the same duration. After 4 weeks, western blotting analysis of three independent groups of 5×FAD littermates revealed that the administration of NSC697923 effectively decreased Aβ dimers levels and suppressed K63 ubiquitination, when compared to the vehicle control (Figure 7B, C). Increased UPS clearance ability, represented by chymotrypsin-like and post-glutamyl activities, was observed following the delivery of NSC697923 into the hippocampus (Figure 7D). Immunohistochemical staining with the Aβ 1-42 antibody also indicated a reduced Aβ plaque area in the 5×FAD mouse treated with NSC697923 (Figure 7E, F).

To better illustrate the potential influence of UBE2N inhibitor on AD pathology caused by Aβ, the transcript sequencing and clustering of bulk RNA-seq was conducted to identify the DEGs in three age-matched littermates: 5×FAD−/−, 5×FAD+/−, and NSC697923-treated 5×FAD+/− mice (Figure S7A, B). Individual transcript analysis of subcluster 4 (green types and brackets) and subcluster 5 (blue types and brackets), extracted from the heatmaps of DEGs, revealed that the up- or down-regulated DEGs in 5×FAD+/− mice were reversed by NSC697923 compared to 5×FAD−/− (Figure S7C). Because 5×FAD+/− mice have been documented to exhibit decreased expression of synaptic proteins,[43–45] we focused on whether NSC697923 could reverse this defect. Indeed, RNAseq analysis revealed a decrease in the expression of certain genes related to synaptic proteins, which could be partially rescued by knocking down *UBE2N* (Figure S7D, E). To support this finding, we performed western blotting analysis of synaptic proteins PSD95 and SNAP25 and found that their decrease in 5×FAD+/− mice could be reversed by NSC697923 (Figure 7G, H).

In summary, elevated UBE2N levels during age-dependent Aβ generation contribute to AD pathology. *UBE2N* overexpression exacerbates Aβ deposition in the 5×FAD mouse brain and the senescent monkey brain, whereas deletion of *UBE2N* reduces Aβ generation and cognitive deficiency. Moreover, pharmacological inhibition of *UBE2N* by NSC697923 ameliorates Aβ pathology in the 5×FAD mouse. Therefore, age-dependent UBE2N appears to be a critical regulator of AD pathology and a potential target for pharmacological interventions in AD drug development (Figure 8).

FIGURE 4 Overexpression of *UBE2N* promotes Aβ generation in the senescent wild-type (WT) monkey brain. (A) Construction of AAV-BRI-Aβ42 virus vector expressing Aβ42 under the ubiquitin C (UBC) promoter. (B) Western blotting analysis of Aβ, UBE2N, and K63 in the cortex region of four WT cynomolgus monkeys after co-injection of AAV-E2N and AAV-Aβ42 into the right-side cortex, or co-injection of AAV-GFP and AAV-Aβ42 into the opposite left-side cortex of the same monkey. The arrow indicates the aggregated or the exogenous BRI-Aβ-42 bands. (C) Quantitative representation of band intensity for 6E10, Aβ 1-42, UBE2N, and K63. Data were obtained from four independent western blotting analyses of cortex tissues of WT monkeys injected with AAV-E2N or AAV-GFP. Data are presented as mean ± SEM and analyzed using unpaired Student's *t*-test ($n = 4$ WT monkeys per group, 7- to 9-years-old, **: $p < 0.01$; *: $p < 0.05$). (D) Immunofluorescent staining of WT cynomolgus monkey cortex injected with AAV-E2N and -Aβ42, or AAV-GFP and -Aβ42 control. Aβ aggregates (red) were detected using 6E10 and Aβ 1–42 antibodies, and the nuclei were stained with DAPI (blue). Scale bars: 100 μm. (E) Quantification of amyloid plaque load area with 6E10 and Aβ 1–42 in the WT monkey cortex expressing AAV-E2N or AAV-GFP, in the right or left cortex respectively. Data are presented as mean ± SEM and analyzed using unpaired Student's *t*-test ($n = 4$ WT monkeys per group, 7- to 9-years-old, **: $p < 0.01$). (F) Immunohistochemical staining with the antibody to Aβ 1-42 revealing Aβ plaques in the hippocampus of old (21–23 years) cynomolgus monkeys after AAV-E2N injection into the right cortex region, but not in the AAV-GFP control (left cortex) or in the AAV-E2N-injected middle-aged (7–9 years) cortex. The dotted line indicates the injecting needle pathway. Scale bar: 500 μm. (G) Western blotting analysis of Aβ, UBE2N, and K63 in the middle (7–9 years) and old (21–23 years) age cortex region of 4 WT cynomolgus monkeys after overexpression of UBE2N or GFP control. The arrow indicates the endogenous Aβ-42 or monomer Aβ bands. (H) Quantitative representation of band intensity for Aβ 1–42, UBE2N, and K63. Data were obtained from the cortex tissues of four WT monkeys injected with AAV-UBE2N and AAV-GFP. Data are presented as mean ± SEM and analyzed using one-way ANOVA with Tukey's test ($n = 4$ monkeys per group, ***: $p < 0.001$; **: $p < 0.01$; *: $p < 0.05$; ns: not significant).

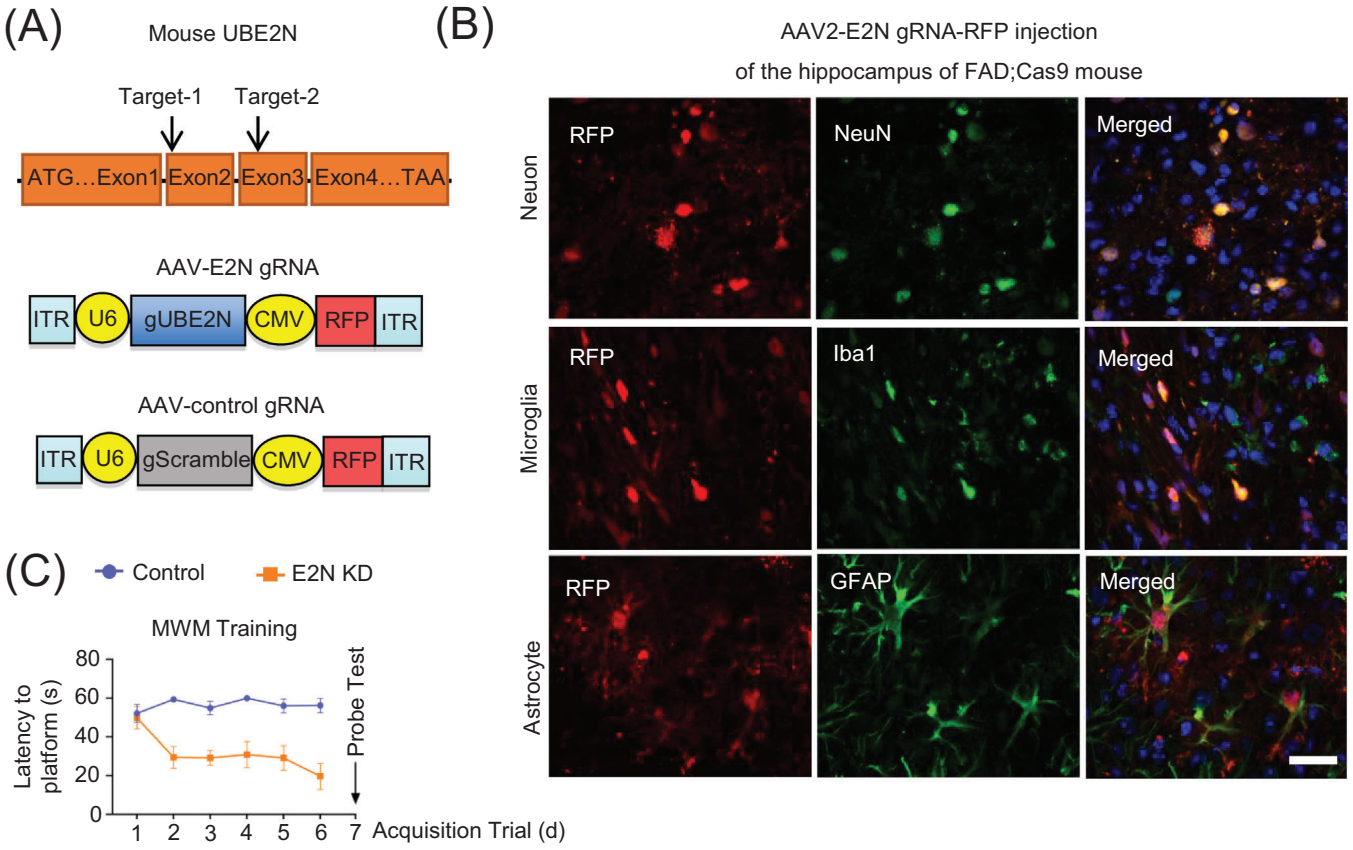

FIGURE 5 Suppression of *UBE2N* reduces cognitive deficiency in the 5×FAD mouse. (A) The guide-RNA targets of the mouse *UBE2N*, which are located in exon 2 or exon 3 sites and are constructed in the AAV2-PX552-red fluorescnet protein (RFP) vector to express E2N gRNA (AAV-gE2N) under the U6 promoter. The RFP fluorescent protein is expressed under the CMV promoter. The scramble sequence of E2N serves as the control (AAV-gCtrl). (B) Identification of different cell types infected by AAV-gE2N-RFP in FAD;Cas9 mice. Immunofluorescent staining of the mouse hippocampus region injected with AAV-gCtrl or AAV-gE2N by antibodies to NeuN (green), GFAP (green), Iba1 (green), and RFP (red). The nuclei were stained with DAPI (blue). The results show the co-expression of NeuN, GFAP, and Iba1 with the guide-RNA in the neuronal and glial cells. Scale bar: 20 μm. (C) Morris water maze test results show the latency time to reach the platform as a readout of spatial memory in 5×FAD;Cas9 mice injected with AAV-gE2N compared to those expressing AAV-gCtrl ($n = 8$ mice per group, 5- to 6-months-old). (D) The swimming speed and the frequency of platform number in the MWM probe test of 5×FAD;Cas9 mice following the injection of AAV-gE2N or AAV-gCtrl. The preference ratio in the novel object recognition test, and the accuracy result in the T-maze test, which reflect memory ability, between AAV-gE2N- and AAV-gCtrl- injected 5×FAD;Cas9 mice. The data are mean ± SEM and were analyzed using an unpaired Student's *t*-test ($n = 8$ mice per group, 5- to 6-months-old, ***: $p < 0.001$, **: $p < 0.01$, *: $p < 0.05$).

4 | DISCUSSION

Age-dependent neurodegenerative diseases, such as AD, Parkinson's disease (PD), and Huntington's disease (HD), are characterized by the accumulation of misfolded proteins, leading to the formation of inclusions in the brain of affected individuals.[14,46–48] The dysfunction of the ubiquitin proteasome system (UPS) is implicated in various neurodegenerative diseases, including AD, PD, and HD.[49,50] There is the closer relationship between Aβ accumulation and impairment of the UPS

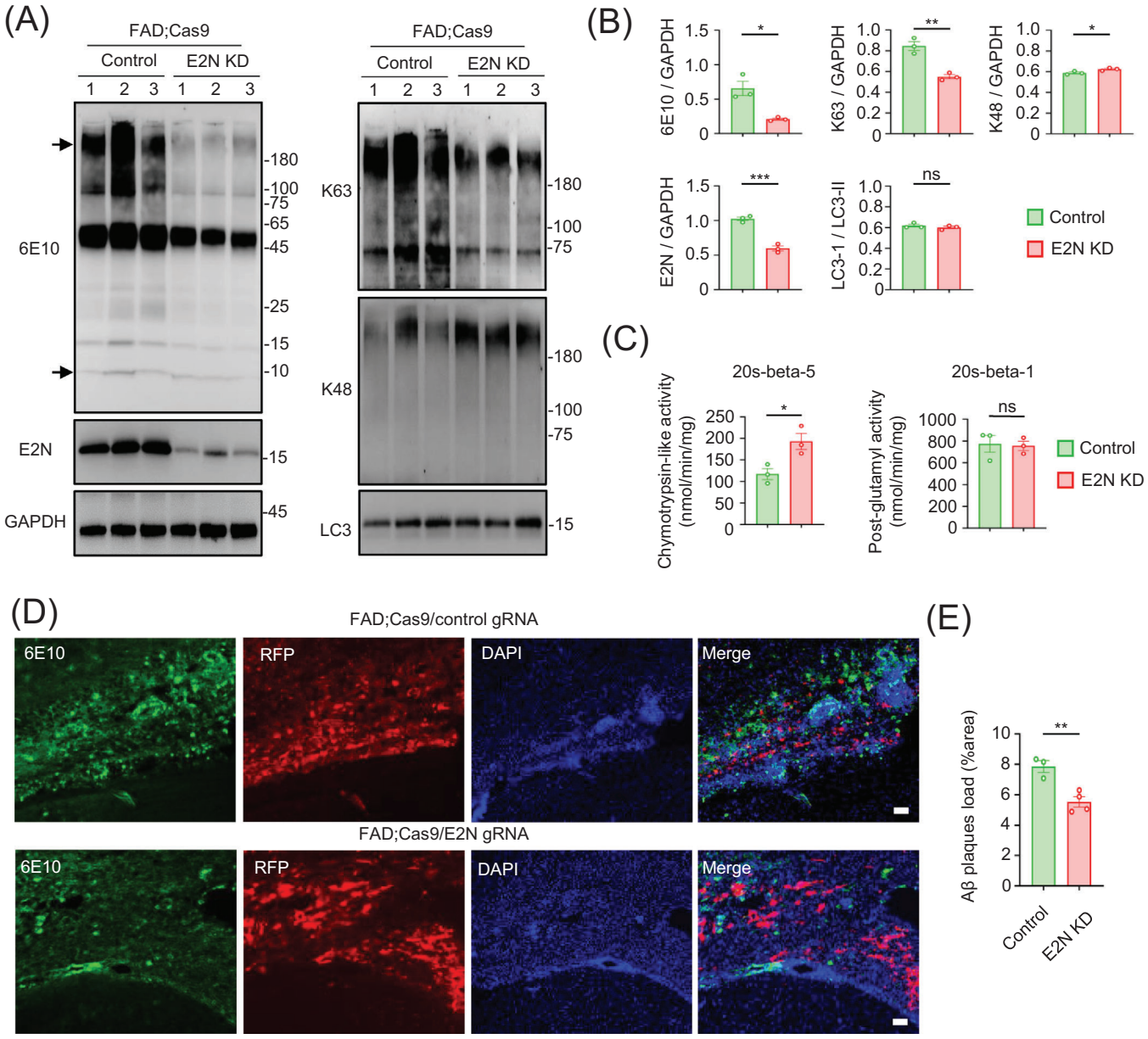

FIGURE 6 Suppression of *UBE2N* alleviates the Aβ pathology in 5×FAD mice. (A) Western blotting analysis of 6E10, UBE2N, K63, K48, and LC3 in two 5×FAD;Cas9 mice injected with AAV-gE2N or AAV-gCtrl. The arrow indicates the aggregated or monomer Aβ bands. (B) Quantitative representation of the band intensity of 6E10, UBE2N, K63, K48, and LC3. The data were obtained from the hippocampus of 5×FAD;Cas9 mice injected with AAV-gE2N and AAV-gCtrl. The data are mean ± SEM and were analyzed using an unpaired Student's *t*-test ($n = 4$ mice per group, 5- to 6-months-old, ***: $p < 0.001$; **: $p < 0.01$; *: $p < 0.05$; ns: not significant). (C) The chymotrypsin-like and post-glutamyl activities (nmol/min/mg protein) in the hippocampus of 5×FAD;Cas9 mice injected with AAV-gE2N or AAV-gCtrl were determined for the 20s-beta-5 and 20s-beta-1 of ubiquitin-proteasome system (UPS). The data are mean ± SEM and were analyzed using an unpaired Student's *t*-test ($n = 4$ mice per group, 5- to 6-months-old, *: $p < 0.05$; ns: not significant). (D) Immunofluorescent staining of the hippocampus region in 5×FAD;Cas9 mice by the injection of AAV-gE2N or AAV-gCtrl. Aβ aggregates (green color) were detected by 6E10 or Aβ 1–42 antibodies, whereas viral infection is indicated by RFP expression (red color). The nuclei were stained with DAPI (blue color). Scale bars: 100 μm. (E) The quantification of the amyloid plaque load area stained by 6E10 antibody, in the hippocampus region of 5×FAD;Cas9 mice expressing AAV-gE2N or AAV-gCtrl. The data are mean ± SEM and were analyzed using an unpaired Student's *t*-test ($n = 4$ mice per group, 5- to 6-months-old, **: $p < 0.01$).

function in AD.[10,51] Numerous studies have highlighted the role of the UPS in clearing intracellular Aβ.[5,6,10,51] During the process of clearance of misfolded proteins by the UPS, ubiquitin is covalently attached to substrate lysine residues through a three-enzyme cascade involving E1 activating enzymes, E2 conjugating enzymes, and E3 ligases.[52] UBE2N, as an E2 conjugating enzyme, selectively mediates the elongation of K63-linked polyubiquitin chains.[23–25]

The increased expression of *UBE2N* has been implicated in various pathological conditions. To date, UBE2N has been mostly characterized as a potential contributor in breast cancer, neuroblastoma, or

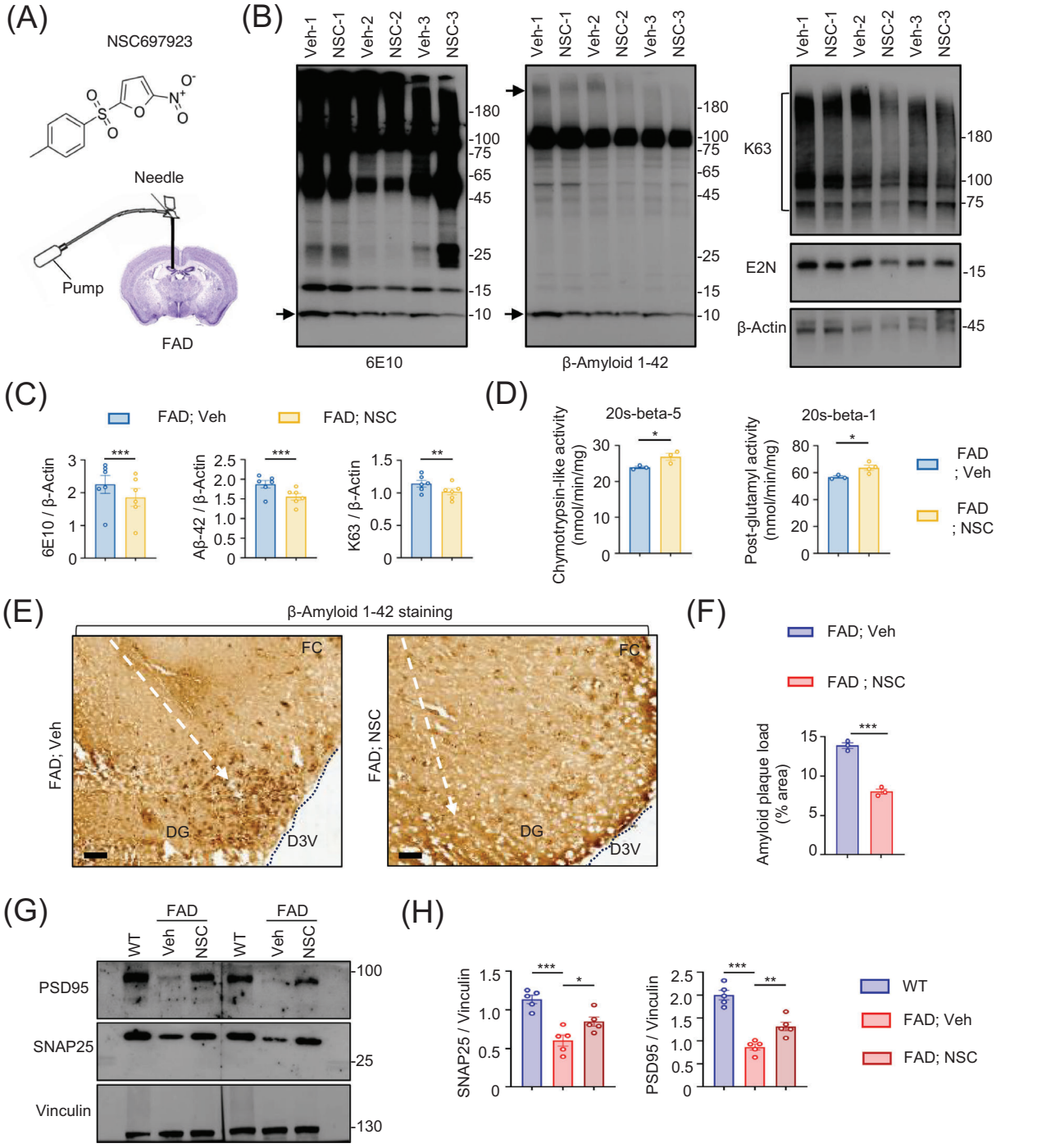

FIGURE 7 Pharmacological inhibition of *UBE2N* by NSC697923 ameliorates Aβ pathology in 5×FAD mice. (A) The chemical structure of UBE2N inhibitor NSC697923 and the schematic diagram for its delivery into the hippocampus of 5×FAD mice through Alzet Pump infusion of 535 ng/100 μL UBE2N inhibitor (NSC, NSC697923+40% PEG300+0.9% NaCl) or the matched vehicle control (Veh, 2% DMSO+40% PEG300+0.9% NaCl), at 0.11 μL/h for 4 weeks. (B) Western blotting analysis of Aβ, UBE2N, and K63 in three independent experiments of 5×FAD mice, administered with the UBE2N inhibitor NSC697923 (NSC) or vehicle control (DMSO). The arrow indicates the aggregated or monomer Aβ bands. (C) Quantitative representation of the band intensity of the aggregated Aβ bands for 6E10, Aβ 1-42 or K63. The data were obtained from the hippocampus of 5×FAD mice, administered with NSC697923 (NSC) or vehicle control (Veh). The data are mean ± SEM and were analyzed using unpaired Student's *t*-test ($n = 6$ mice per group, 5 to 6-months-old, **: $p < 0.01$; ***$p < 0.001$). (D) The chymotrypsin-like and post-glutamyl activities (nmol/min/mg protein) in the hippocampus of 5×FAD mice after delivering the UBE2N inhibitor NSC697923 (NSC) or vehicle control (DMSO) for UPS activity. The data are mean ± SEM and were obtained from three independent experiments, analyzed using an unpaired Student's *t*-test ($n = 6$ mice per group, 5- to 6-months-old, *: $p < 0.05$). (E) Immunohistochemical staining with the antibody to Aβ 1-42 indicates the changed Aβ plaques in the hippocampus of 5×FAD mice after delivering the UBE2N inhibitor NSC697923 (NSC), when compared to the vehicle control (DMSO). The dotted line indicates the needle pathway of the pump administration. Scale bar: 200 μm. (F) Quantitative analysis of the Aβ plaques (the average optical density) of Panel E. Five random fields (20X) in each slice from three animals in each group were used to generate data. The

B-cell lymphoma.[42,53,54] However, in the nervous system, UBE2N has a closer relationship between the UPS and accumulated protein generation, and particularly interferes with the abnormal binding of ubiquitin or its clearance pathway. For examples, *UBE2N* is upregulated in the striatum and hippocampus in methamphetamine-induced neurotoxicity in rats.[55] Knockdown of α-synuclein exacerbates the glutamate neurotoxicity and stimulates *UBE2N* expression.[56] Because UPS activity declines with aging in various tissues,[57–60] we previously identified

data are presented as mean ± SEM, analyzed using unpaired Student's *t*-test (***: $p < 0.001$). (G) Western blotting analysis of PSD95 and SNAP25 in WT, vehicle- 5×FAD+/- (FAD+/-;Veh), and NSC697923- administered 5×FAD+/– (FAD+/-;NSC) mice, showing that the decreased expression of PSD95 and SNAP25 in 5×FAD+/– mice was reversed by the UBE2N inhibitor NSC697923. (H) Quantitative analysis of the intensity of PSD95 and SNAP25 bands. The data were obtained from the mouse hippocampus. The data are mean ± SEM and were analyzed using unpaired Student's *t*-test ($n = 4$ mice per group, 5- to 6-months-old, *: $p < 0.05$; **: $p < 0.01$; ***: $p < 0.001$).

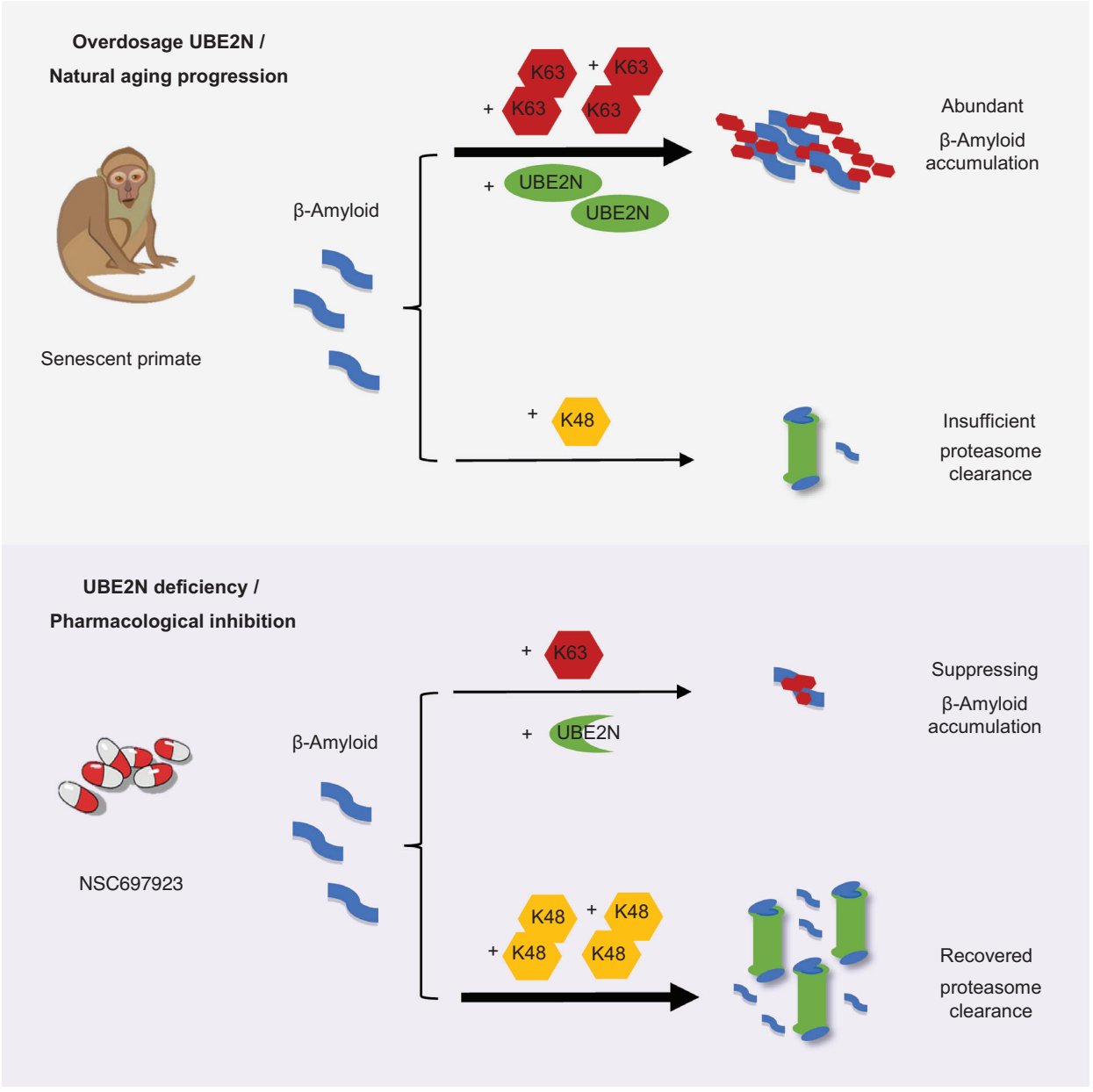

FIGURE 8 A proposed model of the role of aging-related UBE2N as a regulator in AD pathology. UBE2N levels increase during age-dependent Aβ generation in AD pathology. *UBE2N* overexpression exacerbates Aβ deposition in the 5×FAD mouse and senescent monkey brains, whereas *UBE2N* knockdown reduces Aβ generation and cognitive deficiency. Pharmacological inhibition of *UBE2N* using NSC697923 ameliorates Aβ pathology in 5×FAD mouse. The age-dependent increase in UBE2N may worsen AD pathology and could potentially serve as a pharmacological target for AD therapy.

the age-dependent elevated UBE2N and impaired proteasome activity in senescent monkey synaptosomes, which promote the accumulation of misfolded mutant HTT through preferential K63 ubiquitination.[17] In mouse brains, age-dependent increase in UBE2N is also associated with impaired UPS activity and cytoplasmic accumulation of mutant *TDP-43*.[18]

In the current study, we observed the increased *UBE2N* expression during Aβ generation in the brains of 5×FAD mice, APP/PS1 mice, and patients with AD. This finding supports the notion that age-dependent accumulation of pathological proteins results from impaired cellular capacity to clear misfolded proteins.[14–16] Consistently, we found that *UBE2N* overexpression exacerbates Aβ deposition and cognitive deficits in 5×FAD mouse brain, mediated by the K63-linked polyubiquitination. Conversely, suppressing *UBE2N* reduces Aβ generation and improves cognitive behavior, through promoting UPS degradation in mouse brains. Of interest, we found that the elevated UBE2N levels promote the generation of smaller Aβ dimers in the senescent monkey brain through K63 ubiquitin modification. This observation is supported by accumulating data supporting the role of UBE2N in the accumulation of misfolded proteins.[32,33,61–63]

Despite the lack of obvious tauopathy in the AD mice (5×FAD and APP) utilized in our study,[22,64] our investigation of TauP301S mice revealed elevated levels of UBE2N in their brains. This finding aligns with prior research indicating that K63-linked ubiquitination of tau oligomers contributes to AD pathogenesis.[12,13] Old NHPs also exhibit early AD-like pathologies, including Aβ plaque accumulation and cognitive impairment.[28] Diminished cognitive abilities with aging have been demonstrated in several NHP species, including marmosets,[65,66] rhesus macaques,[29–31] and chimpanzees.[67,68] Although tauopathy was found in very old cynomolgus monkeys (>30 years),[37] we observed that overexpression of *UBE2N* selectively increased Aβ rather than phosphorylated tau, suggesting that a longer aging process may be necessary for the development of tau pathology in the primate brains. In addition, given the roles of aging and neuroinflammation in the development of neurodegenerative diseases, further investigations are warranted to explore the potential association of UBE2N with the neuroinflammation in the aged brain.

In our cynomolgus monkey, during the natural aging process, the smaller generated Aβ dimer may have a potential conformation that can be readily ubiquitinated at K63. UBE2N is expressed intracellularly, so that it is plausible that increased levels of UBE2N may impede the intracellular clearance of oligomerized Aβ, potentially augmenting the formation of extracellular amyloid plaques. However, further research is necessary to explore whether soluble or oligomerized Aβ is more susceptible to elevation by an increase in UBE2N.

One of the interesting findings in our study is that the UBE2N inhibitor NSC697923 can slow the development of pathology in AD mice, which is also supported by gene-expression profiling analysis. In 5×FAD mice, which overexpress mutant forms of amyloid precursor protein (or APP) and presenilin-1 (or PS1), changes in synaptic proteins have been observed.[43–45] As for pharmacological inhibitors, the E2N inhibitor NSC697923, delivered into the 5×FAD mice, showed the reversal effects, supporting the involvement of synaptic proteins in AD pathology. Our findings suggest that *UBE2N* inhibition could be an effective drug for alleviating amyloid deposition in AD brain. However, given its multifunctional roles and potential implications in tumors,[42,53] further characterization of the long-term effects and appropriate dosage of UBE2N inhibitors in AD animal models is necessary for validation as an effective anti-AD drug. Taken together, our studies offer additional clues about UBE2N-mediated K63 ubiquitination in the pathological role of Aβ deposition and generation, suggesting a small molecule pharmacological strategy for AD development.

AUTHOR CONTRIBUTIONS

P.Y. and X.-J.L. designed the research. C.Z., Q.J., L.Z., J.H. and X.W. performed the research. D.L. and Y.Z. assisted with the experiments and analysis. J.Z. worked on monkey care and surgery. S.Y. and Z.T. provided AD mouse or tissues. X.Y. provided patients' samples. W.Y. and S.L. provided technical guidance. P.Y., C.Z. and X.-J.L. wrote the article. All the authors reviewed the article.

ACKNOWLEDGMENTS

The authors thank all members of the Li laboratory for helpful discussions, and the staff working at Jinan University and Guangdong Landao Co. Ltd. for animal care and experiment. This work was supported by the National Natural Science Foundation of China (32270564, 82394422, 82371874, 82271902, 82071421, 31500826); the Guangzhou Key Research Program on Brain Science (202007030008); the Department of Science and Technology of Guangdong Province (2021ZT09Y007, 2018B030337001); and the Guangdong Basic and Applied Basic Research (2022A1515011205, 2023A1515010811).

CONFLICT OF INTEREST STATEMENT

The authors have declared that there are no conflicts of interest. Author disclosures are available in the supporting information.

CONSENT STATEMENT

All human subjects have written the informed consent.

INCLUSION AND DIVERSITY

We support inclusive, diverse, and equitable conduct of research.

REFERENCES

1. Xia X, Jiang Q, McDermott J, Han JJ. Aging and Alzheimer's disease: comparison and associations from molecular to system level. *Aging Cell*. 2018;17:e12802.
2. Hou Y, Dan X, Babbar M, et al. Ageing as a risk factor for neurodegenerative disease. *Nat Rev Neurol*. 2019;15:565-581.
3. Braak H, Del Tredici K. The pathological process underlying Alzheimer's disease in individuals under thirty. *Acta Neuropathol*. 2011;121:171-181.
4. DeTure MA, Dickson DW. The neuropathological diagnosis of Alzheimer's disease. *Molecular neurodegeneration*. 2019;14:32.
5. Hong L, Huang HC, Jiang ZF. Relationship between amyloid-beta and the ubiquitin-proteasome system in Alzheimer's disease. *Neurol Res*. 2014;36:276-282.
6. Oddo S. The ubiquitin-proteasome system in Alzheimer's disease. *J Cell Mol Med*. 2008;12:363-373.

7. El Ayadi A, Stieren ES, Barral JM, Boehning D. Ubiquilin-1 regulates amyloid precursor protein maturation and degradation by stimulating K63-linked polyubiquitination of lysine 688. *Proc Nat Acad Sci USA*. 2012;109:13416-13421.
8. Duggan SP, Yan R, McCarthy JV. A ubiquitin-binding CUE domain in presenilin-1 enables interaction with K63-linked polyubiquitin chains. *FEBS Lett*. 2015;589:1001-1008.
9. Paine S, Bedford L, Thorpe JR, et al. Immunoreactivity to Lys63-linked polyubiquitin is a feature of neurodegeneration. *Neurosci Lett*. 2009;460:205-208.
10. Bellia F, Lanza V, García-Viñuales S, et al. Ubiquitin binds the amyloid β peptide and interferes with its clearance pathways. *Chem Sci*. 2019;10:2732-2742.
11. Morimoto D, Walinda E, Fukada H, et al. The unexpected role of polyubiquitin chains in the formation of fibrillar aggregates. *Nat Commun*. 2015;6:6116.
12. Puangmalai N, Sengupta U, Bhatt N, et al. Lysine 63-linked ubiquitination of tau oligomers contributes to the pathogenesis of Alzheimer's disease. *J Biol Chem*. 2022;298:101766.
13. Tan JM, Wong ES, Kirkpatrick DS, et al. Lysine 63-linked ubiquitination promotes the formation and autophagic clearance of protein inclusions associated with neurodegenerative diseases. *Hum Mol Genet*. 2008;17:431-439.
14. Douglas PM, Dillin A. Protein homeostasis and aging in neurodegeneration. *J Cell Biol*. 2010;190:719-729.
15. Rubinsztein DC. The roles of intracellular protein-degradation pathways in neurodegeneration. *Nature*. 2006;443:780-786.
16. Tai HC, Schuman EM. Ubiquitin, the proteasome and protein degradation in neuronal function and dysfunction. *Nat Rev Neurosci*. 2008;9:826-838.
17. Yin P, Tu Z, Yin A, et al. Aged monkey brains reveal the role of ubiquitin-conjugating enzyme UBE2N in the synaptosomal accumulation of mutant huntingtin. *Hum Mol Genet*. 2015;24:1350-1362.
18. Yin P, Bai D, Zhu L, et al. Cytoplasmic TDP-43 impairs the activity of the ubiquitin-proteasome system. *Exp Neurol*. 2021;345:113833.
19. Qiu W, Zhang H, Bao A, et al. Standardized Operational Protocol for Human Brain Banking in China. *Neuroscience bulletin*. 2019;35:270-276.
20. Yan X-X, Ma C, Bao A-M, Wang X-M, Gai W-P. Brain banking as a cornerstone of neuroscience in China. *The Lancet Neurology*. 2015;14:136.
21. Christensen A, Pike CJ. Staining and quantification of β-amyloid pathology in transgenic mouse models of Alzheimer's disease. *Aging: Methods and Protocols*. 2020:211-221.
22. Maarouf CL, Kokjohn TA, Whiteside CM, et al. Molecular differences and similarities between Alzheimer's disease and the 5XFAD transgenic mouse model of amyloidosis. *Biochemistry insights*. 2013;6:S13025. BCI.
23. Chang JH, Xiao Y, Hu H, et al. Ubc13 maintains the suppressive function of regulatory T cells and prevents their conversion into effector-like T cells. *Nat Immunol*. 2012;13:481-490.
24. Sato M, Konuma R, Sato K, Tomura K, Sato K. Fertilization-induced K63-linked ubiquitylation mediates clearance of maternal membrane proteins. *Development*. 2014;141:1324-1331.
25. Wu X, Yamamoto M, Akira S, Sun SC. Regulation of hematopoiesis by the K63-specific ubiquitin-conjugating enzyme Ubc13. *Proc Nat Acad Sci USA*. 2009;106:20836-20841.
26. Yamaguchi F, Richards SJ, Beyreuther K, Salbaum M, Carlson GA, Dunnett SB. Transgenic mice for the amyloid precursor protein 695 isoform have impaired spatial memory. *Neuroreport*. 1991;2:781-784.
27. Chen G, Chen KS, Knox J, et al. A learning deficit related to age and β-amyloid plaques in a mouse model of Alzheimer's disease. *Nature*. 2000;408:975-979.
28. Freire-Cobo C, Edler MK, Varghese M, et al. Comparative neuropathology in aging primates: a perspective. *Am J Primatol*. 2021;83:e23299.
29. Moss MB, Rosene DL, Peters A. Effects of aging on visual recognition memory in the rhesus monkey. *Neurobiol Aging*. 1988;9:495-502.
30. Herndon JG, Moss MB, Rosene DL, Killiany RJ. Patterns of cognitive decline in aged rhesus monkeys. *Behav Brain Res*. 1997;87:25-34.
31. Fukumoto H, Rosene DL, Moss MB, Raju S, Hyman BT, Irizarry MC. Beta-secretase activity increases with aging in human, monkey, and mouse brain. *Am J Pathol*. 2004;164:719-725.
32. Frye BM, Craft S, Latimer CS, et al. Aging-related Alzheimer's disease-like neuropathology and functional decline in captive vervet monkeys (Chlorocebus aethiops sabaeus). *Am J Primatol*. 2021;83:e23260.
33. Latimer CS, Shively CA, Keene CD, et al. A nonhuman primate model of early Alzheimer's disease pathologic change: implications for disease pathogenesis. *Alzheimer's & dementia : the journal of the Alzheimer's Association*. 2019;15:93-105.
34. Chen JA, Fears SC, Jasinska AJ, et al. Neurodegenerative disease biomarkers Aβ(1-40), Aβ(1-42), tau, and p-tau(181) in the vervet monkey cerebrospinal fluid: relation to normal aging, genetic influences, and cerebral amyloid angiopathy. *Brain and behavior*. 2018;8:e00903.
35. Frye BM, Valure PM, Craft S, et al. Temporal emergence of age-associated changes in cognitive and physical function in vervets (Chlorocebus aethiops sabaeus). *GeroScience*. 2021;43:1303-1315.
36. Frye BM, Craft S, Register TC, et al. Early Alzheimer's disease-like reductions in gray matter and cognitive function with aging in non-human primates. *Alzheimer's & dementia (New York, N Y)*. 2022;8:e12284.
37. Uchihara T, Endo K, Kondo H, et al. Tau pathology in aged cynomolgus monkeys is progressive supranuclear palsy/corticobasal degeneration-but not Alzheimer disease-like-Ultrastructural mapping of tau by EDX. *Acta Neuropathologica Communications*. 2016;4:1-13.
38. Grice GL, Nathan JA. The recognition of ubiquitinated proteins by the proteasome. Cellular and molecular life sciences. *CMLS*. 2016;73:3497-3506.
39. Elofsson M, Splittgerber U, Myung J, Mohan R, Crews CM. Towards subunit-specific proteasome inhibitors: synthesis and evaluation of peptide alpha',beta'-epoxyketones. *Chem Biol*. 1999;6:811-822.
40. Hodge CD, Edwards RA, Markin CJ, et al. Covalent inhibition of Ubc13 affects ubiquitin signaling and reveals active site elements important for targeting. *ACS Chem Biol*. 2015;10:1718-1728.
41. Gombodorj N, Yokobori T, Yoshiyama S, et al. Inhibition of ubiquitin-conjugating enzyme E2 may activate the degradation of hypoxia-inducible factors and, thus, overcome cellular resistance to radiation in colorectal cancer. *Anticancer Res*. 2017;37:2425-2436.
42. Cheng J, Fan YH, Xu X, et al. A small-molecule inhibitor of UBE2N induces neuroblastoma cell death via activation of p53 and JNK pathways. *Cell Death Dis*. 2014;5:e1079.
43. Oakley H, Cole SL, Logan S, et al. Intraneuronal β-amyloid aggregates, neurodegeneration, and neuron loss in transgenic mice with five familial Alzheimer's disease mutations: potential factors in amyloid plaque formation. *J Neurosci*. 2006;26:10129-10140.
44. van der Spek SJ, Gonzalez-Lozano MA, Koopmans F, et al. Age-dependent hippocampal proteomics in the APP/PS1 alzheimer mouse model: a comparative analysis with classical SWATH/DIA and direct-DIA approaches. *Cells*. 2021;10:1588.
45. Cai H, Pang Y, Ren Z, Fu X, Jia L. Delivering synaptic protein mRNAs via extracellular vesicles ameliorates cognitive impairment in a mouse model of Alzheimer's disease. *BMC medicine*. 2024;22:138.
46. Benilova I, Karran E, De Strooper B. The toxic Aβ oligomer and Alzheimer's disease: an emperor in need of clothes. *Nat Neurosci*. 2012;15:349-357.
47. Irwin DJ, Lee VM, Trojanowski JQ. Parkinson's disease dementia: convergence of α-synuclein, tau and amyloid-β pathologies. *Nat Rev Neurosci*. 2013;14:626-636.
48. Li XJ, Li S. Proteasomal dysfunction in aging and Huntington disease. *Neurobiol Dis*. 2011;43:4-8.

49. Liu B, Ruan J, Chen M, et al. Deubiquitinating enzymes (DUBs): decipher underlying basis of neurodegenerative diseases. *Mol Psychiatry*. 2022;27:259-268.
50. Zheng Q, Huang T, Zhang L, et al. Dysregulation of Ubiquitin-Proteasome System in Neurodegenerative Diseases. *Front Aging Neurosci*. 2016;8:303.
51. Riederer BM, Leuba G, Vernay A, Riederer IM. The role of the ubiquitin proteasome system in Alzheimer's disease. *Experimental biology and medicine (Maywood, NJ)*. 2011;236:268-276.
52. Kerscher O, Felberbaum R, Hochstrasser M. Modification of proteins by ubiquitin and ubiquitin-like proteins. *Annu Rev Cell Dev Biol*. 2006;22:159-180.
53. Pulvino M, Liang Y, Oleksyn D, et al. Inhibition of proliferation and survival of diffuse large B-cell lymphoma cells by a small-molecule inhibitor of the ubiquitin-conjugating enzyme Ubc13-Uev1A. *Blood, The Journal of the American Society of Hematology*. 2012;120:1668-1677.
54. Wu X, Zhang W, Font-Burgada J, et al. Ubiquitin-conjugating enzyme Ubc13 controls breast cancer metastasis through a TAK1-p38 MAP kinase cascade. *Proceed Natl Acad Sci USA*. 2014;111:13870-13875.
55. Li X, Wang H, Qiu P, Luo H. Proteomic profiling of proteins associated with methamphetamine-induced neurotoxicity in different regions of rat brain. *Neurochem Int*. 2008;52:256-264.
56. Leng Y, Chuang DM. Endogenous alpha-synuclein is induced by valproic acid through histone deacetylase inhibition and participates in neuroprotection against glutamate-induced excitotoxicity. The Journal of neuroscience : the official journal of the Society for. *Neuroscience*. 2006;26:7502-7512.
57. Kapphahn RJ, Bigelow EJ, Ferrington DA. Age-dependent inhibition of proteasome chymotrypsin-like activity in the retina. *Exp Eye Res*. 2007;84:646-654.
58. Keller JN, Hanni KB, Markesbery WR. Possible involvement of proteasome inhibition in aging: implications for oxidative stress. *Mech Ageing Dev*. 2000;113:61-70.
59. Löw P. The role of ubiquitin-proteasome system in ageing. *Gen Comp Endocrinol*. 2011;172:39-43.
60. Tydlacka S, Wang CE, Wang X, Li S, Li XJ. Differential activities of the ubiquitin-proteasome system in neurons versus glia may account for the preferential accumulation of misfolded proteins in neurons. *The Journal of neuroscience : the official journal of the Society for Neuroscience*. 2008;28:13285-13295.
61. Chen X, Errangi B, Li L, et al. Brain aging in humans, chimpanzees (Pan troglodytes), and rhesus macaques (Macaca mulatta): magnetic resonance imaging studies of macro- and microstructural changes. *Neurobiol Aging*. 2013;34:2248-2260.
62. Mulholland MM, Sherwood CC, Schapiro SJ, Raghanti MA, Hopkins WD. Age- and cognition-related differences in the gray matter volume of the chimpanzee brain (Pan troglodytes): a voxel-based morphometry and conjunction analysis. *Am J Primatol*. 2021;83:e23264.
63. Andersen AH, Zhang Z, Zhang M, Gash DM, Avison MJ. Age-associated changes in rhesus CNS composition identified by MRI. *Brain Res*. 1999;829:90-98.
64. Jackson RJ, Rudinskiy N, Herrmann AG, et al. Human tau increases amyloid β plaque size but not amyloid β-mediated synapse loss in a novel mouse model of Alzheimer's disease. *Eur J Neurosci*. 2016;44:3056-3066.
65. Workman KP, Healey B, Carlotto A, Lacreuse A. One-year change in cognitive flexibility and fine motor function in middle-aged male and female marmosets (Callithrix jacchus). *Am J Primatol*. 2019;81:e22924.
66. Sadoun A, Rosito M, Fonta C, Girard P. Key periods of cognitive decline in a nonhuman primate model of cognitive aging, the common marmoset (Callithrix jacchus). *Neurobiol Aging*. 2019;74:1-14.
67. Lacreuse A, Parr L, Chennareddi L, Herndon JG. Age-related decline in cognitive flexibility in female chimpanzees. *Neurobiol Aging*. 2018;72:83-88.
68. Hopkins WD, Mareno MC, Neal Webb SJ, Schapiro SJ, Raghanti MA, Sherwood CC. Age-related changes in chimpanzee (Pan troglodytes) cognition: cross-sectional and longitudinal analyses. *Am J Primatol*. 2021;83:e23214.

SUPPORTING INFORMATION

Additional supporting information can be found online in the Supporting Information section at the end of this article.

How to cite this article: Zhang C, Jia Q, Zhu L, et al. Suppressing *UBE2N* ameliorates Alzheimer's disease pathology through the clearance of amyloid beta. *Alzheimer's Dement*. 2024;20:6287–6304. https://doi.org/10.1002/alz.14122